ELSEVIER

Advances in Water Resources 23 (2000) 359–372

Advances in Water Resources

A two-dimensional finite element drying-wetting shallow water model for rivers and estuaries

Mourad Heniche *, Yves Secretan, Paul Boudreau, Michel Leclerc

Institut National de la Recherche Scientifique-Eau, 2800 Einstein St., Suite 105, P.O.B.7500, Sainte-Foy(Qc), Canada, G1V 4C7

Received 20 September 1998; received in revised form 20 June 1999; accepted 1 July 1999

Abstract

A new finite element model has been developed to simulate two-dimensional free surface flow in rivers and estuaries. The variables of the model are the specific discharge and the water level. The algorithm takes into account the natural boundaries of the flow, defined by the contour lines of zero depth, with a new approach that accepts positive and negative values for the water depth. In this way, we consider a wet or dry area when the water depth is positive or negative respectively. A 6-node triangular element and an implicit Euler scheme are respectively used for spatial and time discretization of the mathematical model. The solution procedure is based on the inexact Newton-GMRES type solver with incomplete factorization as preconditioning. The numerical results of the proposed approach are in good agreement with an analytic solution and also with the classical approach. © 2000 Elsevier Science Ltd. All rights reserved.

Keywords: Conservative form; Free surface flow; Mixed finite element; Moving boundary; Shallow water

1. Introduction

In modeling hydrodynamics of rivers and estuaries, it is important to have a robust approach capable of reproducing moving shorelines which are boundaries separating dry and wet areas. A review of several approaches [4,10,13,18,25] for the representation of the moving boundary is given by Leclerc et al. [17]. One of the approaches considered in this study for comparison and referred to as the classical approach was presented by Leclerc et al. [17] and Zhang et al. [25] It is based on an Eulerian description with a fixed spatial mesh. The solution procedure in predicting the position of the moving boundary distinguishes wet, dry and partially wet or transition elements. The nodes are free and the governing equations are entirely solved in wet elements. For the dry elements, the nodes are locked; in other words, the velocity is assumed equal to zero and the water level is fixed at the bed level (Fig. 1a). In transition elements, the equations of momentum are partially solved by dropping out advection and artificial slope of the free surface. The term '*artificial*' is employed because on the dry nodes, the water level is arbitrarily fixed at the bed level; thus the resulting slope of the free surface is fictitious. Hence, in the finite element assembly procedure, it becomes essential to recognize and to compute separately wet, dry and transition elements. Moreover, in the transition elements it is requested to distinguish between draining and filling elements in order to either lock or free the dry nodes. Although this method is robust, the several diagnostic tests above complicate its implementation in a finite element code, particularly with an iterative type solver.

In this paper, a new technique in Eulerian form is proposed. Its originality resides in its adaptability and ease of programming. It was successfully used in studying stationary and nonstationary real flow cases. The new approach is also based on an Eulerian description with a fixed spatial mesh, but we do not presume or test anything on the water level position. Thus the Saint–Venant equations are solved on the entire domain of simulation. By letting the water level free to plunge under the bed level, positive and negative water depth values may be encountered (Fig. 1b). Physically, a negative depth does not make sense; as a consequence, a flow in the dry area would cause an artificial mass transfer from the dry to the wet area and vice versa, which would change the characteristics of the flow. Therefore, to satisfy mass and momentum conservation

* Corresponding author.

0309-1708/00/$ - see front matter © 2000 Elsevier Science Ltd. All rights reserved.
PII: S0309-1708(99)00031-7

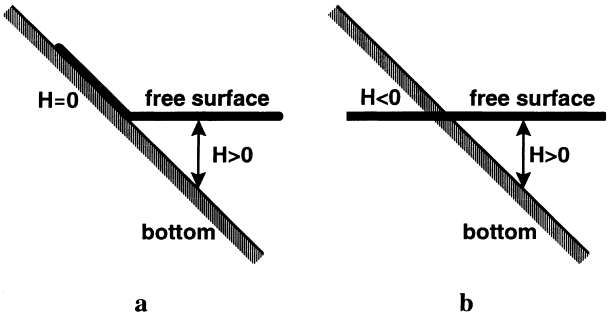

Fig. 1. Representation of moving boundary: (a) classical approach; (b) new approach.

in the wet area, the flow in the dry area, powered by the slope of the free surface, is frozen in order to have zero discharge conditions. This method was applied by Ghanem [8], simultaneously using a modification of the Saint–Venant equations in the dry area in order to obtain an analogous model for underground flow.

In the present study, the main objective is to present in detail the finite element model for the two-dimensional free surface flow for shallow water problems, using the new Eulerian method to predict the position of the moving boundary. In the next sections, the equations of Saint–Venant in conservative form for moving boundaries are presented. A 6-node triangular finite element is used to discretize the mathematical model. The variables of the model are the specific discharge and the water level. Linear and piecewise linear spatial approximations for water level and specific discharge, to satisfy the Brezzi–Babuska compatibility condition, and a fully implicit Euler scheme for temporal approximations are employed. The resulting nonlinear algebraic system is solved by an inexact Newton procedure. The methodology followed and the results obtained are presented next.

2. Governing equations

2.1. Shallow water equations

Modeling 2D hydrodynamics in rivers and estuaries requires the local prediction of the water depth, mean velocities in the vertical direction, and position of wet and dry areas for a given event (discharge). To that purpose, we use an adaptation of the incompressible Navier–Stokes equations by assuming the following:

- the water column is well mixed in the vertical direction and the depth is small in comparison with the horizontal width;
- the waves are of small amplitude and of long period (tidal waves). The vertical component of the acceleration is negligible, permitting a hydrostatic pressure approximation;
- the velocity is assumed constant in the vertical direction;
- the porosity of the field is taken into account to make the difference between wet and dry area which is explained further along the presentation of the drying-wetting model in Section 4.

Taking into account the key points cited above, the Reynolds-averaged three-dimensional incompressible Navier–Stokes equations for turbulent flow are integrated in the vertical component z to give the well-known two-dimensional equations of Saint–Venant [4,12,19] for shallow water problems. These equations governing the mass and momentum conservation can be written in conservative form [10,15], with specific discharge $\boldsymbol{q}(q_x,q_y)$ and water level h as variables, as follows, for mass conservation

$$\frac{\partial pH}{\partial t}+\frac{\partial q_x}{\partial x}+\frac{\partial q_y}{\partial y}=0 \tag{1}$$

and momentum conservation

$$\begin{aligned}
&\frac{\partial (pq_x)}{\partial t}+\frac{\partial}{\partial x}\left(\frac{q_xq_x}{H}\right)+\frac{\partial}{\partial y}\left(\frac{q_xq_y}{H}\right)+c^2\frac{\partial h}{\partial x}\\
&\qquad -\frac{1}{\rho}\left(\frac{\partial}{\partial x}(H\tau_{xx})+\frac{\partial}{\partial y}(H\tau_{xy})-\tau_x^{\mathrm{b}}+\tau_x^{P}\mathrm{s}\right)-f_{\mathrm{c}}q_y=0,\\
&\frac{\partial (pq_y)}{\partial t}+\frac{\partial}{\partial x}\left(\frac{q_yq_x}{H}\right)+\frac{\partial}{\partial y}\left(\frac{q_yq_y}{H}\right)+c^2\frac{\partial h}{\partial y}\\
&\qquad -\frac{1}{\rho}\left(\frac{\partial}{\partial x}(H\tau_{yx})+\frac{\partial}{\partial y}(H\tau_{yy})-\tau_y^{\mathrm{b}}+\tau_y^{\mathrm{s}}\right)+f_{\mathrm{c}}q_x=0,
\end{aligned} \tag{2}$$

where $\boldsymbol{x}(x,y)$ are the Cartesian components, t is the time, p the porosity, g the gravitational acceleration, c the celerity of waves ($c=\sqrt{gH}$), and ρ is the density of the water. We denote by $H(=h-z_{\mathrm{f}})$ the water depth, where h and z_{f} are, respectively, the water surface level and the bed level with respect to a reference plane (Fig. 2). The velocity components $\boldsymbol{u}(u,v)$ are then expressed as

$$u=q_x/H \quad \text{and} \quad v=q_y/H. \tag{3}$$

Generally, the effect of the Coriolis force must be taken into account in the case of great lakes, wide rivers and estuaries. The Coriolis factor f_{c} is given by

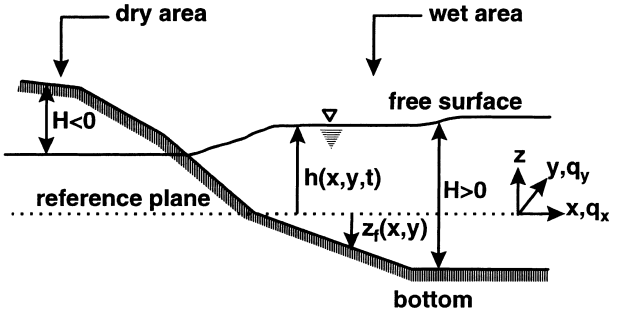

Fig. 2. Shallow water free surface flow with dry and wet area.

$$f_c = 2\omega \sin\phi, \tag{4}$$

where ω is the rotational rate of the earth and ϕ is the latitude of the site under study.

The stress components $\tau_x(\tau_{xx}, \tau_{xy})$ and $\tau_y(\tau_y, \tau_{yy})$ acting on the horizontal plane are the combination of the molecular and Reynolds stresses as follows:

$$\frac{1}{\rho}\begin{bmatrix}\tau_x \\ \tau_y\end{bmatrix} = \frac{1}{\rho}\begin{bmatrix}\tau_{xx} & \tau_{xy} \\ \tau_{yx} & \tau_{yy}\end{bmatrix} = (v + v_t)\begin{bmatrix}2\frac{\partial u}{\partial x} & \left(\frac{\partial u}{\partial y} + \frac{\partial v}{\partial x}\right) \\ \text{sym} & 2\frac{\partial v}{\partial y}\end{bmatrix}, \tag{5}$$

where v is the molecular kinematic viscosity of the water. The turbulent kinematic viscosity v_t, in the sense of Boussinesq (the turbulence of the flow is related to a mean velocity gradient by a constant of proportionality called the eddy or turbulent viscosity, v_t), can have a constant value or may depend on the flow gradient [19]

$$v_t = l_m^2\sqrt{2\left(\frac{\partial u}{\partial x}\right)^2 + 2\left(\frac{\partial v}{\partial y}\right)^2 + \left(\frac{\partial u}{\partial y} + \frac{\partial v}{\partial x}\right)^2} \text{ with } l_m = \lambda H \tag{6}$$

where l_m is the mixing length and λ a calibration coefficient.

The surface stresses τ_x^s and τ_y^s are acting on the wet area only, as there is no wind under the ground. The differentiation is achieved via the porosity p. As usual, the stresses are expressed as the product between a friction coefficient and a quadratic form of the wind velocity

$$\frac{\tau_x^s}{\rho} = C_f^s|w|w_x \quad \text{and} \quad \frac{\tau_y^s}{\rho} = C_f^s|w|w_y \quad \text{with} \quad C_f^s = pc_w\left(\frac{\rho_{air}}{\rho}\right), \tag{7}$$

where $w(w_x, w_y)$ is the velocity of the wind and c_w, the friction coefficient of the wind as proposed by Wu [22]:

$$c_w = 1.25 \times 10^{-3} w^{-1/5} \text{ if } |w| < 1.0 \text{ m/s},$$
$$c_w = 0.50 \times 10^{-3} w^{1/2} \text{ if } 1.0 \text{ m/s} \leqslant |w| < 150 \text{ m/s}, \tag{8}$$
$$c_w = 2.60 \times 10^{-3} \text{ if } |w| \geqslant 15.0 \text{ m/s}$$

and ρ_{air} is the density of the air. For the bottom stresses τ_x^b and τ_y^b, the Chézy–Manning formula is extended to two dimensions to give

$$\frac{\tau_x^b}{\rho} = -C_f^b|q|q_x \quad \text{and} \quad \frac{\tau_y^b}{\rho} = -C_f^b|q|q_y \quad \text{with} \quad C_f^b = \frac{n^2 g}{H^{7/3}}, \tag{9}$$

where n is the Manning coefficient. It defines resistance to flow by various factors such as bottom (subscript b), macrophytes (m) and ice (i)

$$n^2 = n_b^2 + n_m^2 + n_i^2. \tag{10}$$

In practice, excluding macrophytes and ice effects, the Manning coefficient varies generally from 0.02 for a smooth bed (sand) to 0.05 for a rough bed (rocks) [12]. For all examples presented here, where the Coriolis force and the wind stresses are neglected, the values of the physical constants used are given in Table 1.

2.2. Boundary and initial conditions

For natural flows we encounter two types of boundaries (Fig. 3).

2.3. Solid boundary Γ_s

On solid boundary Γ_s a condition on either $\boldsymbol{q}$ or its derivatives (i.e., the stresses) must be imposed. Generally, for realistic flow, one of the two following conditions are retained:

- adherence: normal discharge $q_n = 0$ and tangential discharge $q_t = 0$ on Γ_s;
- friction: normal discharge $q_n = 0$ for impermeability and $\tau_{nt} = f_t$ for tangential stress on Γ_s.

A tangential stress f_t condition is used when the small boundary is neglected to save computational cost; otherwise a mesh refinement would be required in the boundary layer. A slip condition would be for $f_t = 0$. Here we have

$\boldsymbol{q}(q_n, q_t)$: specific discharge in local components $(\boldsymbol{n},\boldsymbol{t})$
$\bar{\bar{\tau}}(\tau_{nn}, \tau_{nt})$: projection of $\bar{\bar{\tau}}$ (5), in local components, on the outward normal to Γ.

Table 1
Values of the physical constant

g (m/s^2)	ρ (kg/m^3)	v (m^2/s)	ρ_{air}(kg/m^3)	ω (rad/s)
9.806	1000	10^{-6}	1.2475	0.7292×10^{-4}

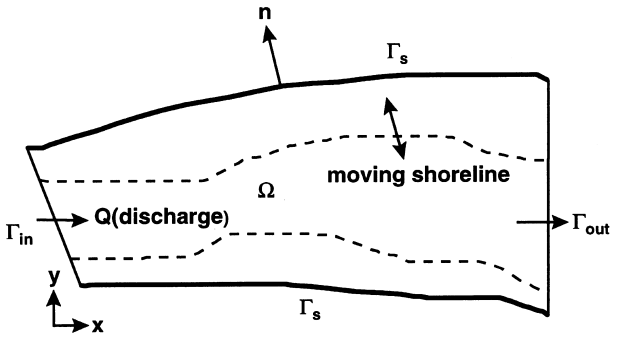

Fig. 3. Definition of the computational domain.

2.4. Open boundaries Γ_{in} and Γ_{out}

The open boundaries are employed to specify the flow regime. Thus the choice of boundary conditions depends to a great extent on the availability of the experimental data. The water surface level h has to be imposed

- $h = h$ on Γ_{in} and Γ_{out}.

Moreover, one can impose the components of q or the distribution of normal f_n and tangential f_t stresses:

- $q_n = \bar{q}_n$ or $\tau_{nn} = f_n$ on Γ_{in} and Γ_{out};
- $q_t = \bar{q}_t$ or $\tau_{nt} = f_t$ on Γ_{in} and Γ_{out}.

The stresses f_n and f_t are often used in order to introduce a friction law on Γ. In our study, we chose for $\bar{f}$ the expression given by (5). The specific aspect of boundary conditions will be discussed further along with the presentation of the formulation used.

For initial conditions, it is important to start from a physical situation, which respects impermeability and mass conservation at least, on the whole computational domain. For a first simulation, it is possible to specify a hydrostatic solution ($\mathbf{q} = \mathbf{0}$ and $h =$ constant) or to specify a spatially variable free surface $h = h(x, y, t_0)$ and in addition to freeze the flow ($\mathbf{q} = \mathbf{0}$).

3. Weak variational formulation

The finite element method is used to discretize the equations of conservation (1) and (2) in order to find q and h and the natural boundaries of the flow, defined by the moving shorelines where we have the zero depth situation (Fig. 3), satisfying the boundary conditions and the initial conditions. The solution is sought on a domain Ω with boundary $\Gamma(=\Gamma_s \cup \Gamma_{in} \cup \Gamma_{out})$ and where $n(n_x,n_y)$ denotes the outward normal to Γ. The standard mixed Galerkin weak variational formulation is used. Multiplying equations of conservation (1) and (2) with arbitrary test functions Φ and $\Psi(\psi_x, \psi_y)$ and integrating by parts the divergence term

$$\left(\frac{\partial q_x}{\partial x} + \frac{\partial q_y}{\partial y}\right)$$

of W_h as well as the second order terms

$$\left(\frac{\partial}{\partial x}(H\tau_{xx}) + \frac{\partial}{\partial y}(H\tau_{xy})\right)$$

of W_{q_x} and

$$\left(\frac{\partial}{\partial x}(H\tau_{yx}) + \frac{\partial}{\partial y}(H\tau_{yy})\right)$$

of W_{q_y} we obtain the following weak forms:

$$W_h = \int_\Omega \Phi \frac{\partial pH}{\partial t}\,\mathrm{d}\Omega - \int_\Omega \left(\frac{\partial \Phi}{\partial x} q_x + \frac{\partial \Phi}{\partial y} q_y\right)\mathrm{d}\Omega + \int_\Gamma \Phi(q_x n_x + q_y n_y)\,\mathrm{d}\Gamma = 0, \tag{11}$$

$$W_{q_x} = \int_\Omega \psi_x \left(\frac{\partial (pq_x)}{\partial t} + \frac{\partial}{\partial x}\left(\frac{q_x q_x}{H}\right) + \frac{\partial}{\partial y}\left(\frac{q_x q_y}{H}\right) + c^2 \frac{\partial h}{\partial y} + C_f^b |q| q_x - C_f^s |w| w_x - f_c q_y\right)\mathrm{d}\Omega + \frac{1}{\rho}\int_\Omega H\left(\frac{\partial \psi_x}{\partial x}\tau_{xx} + \frac{\partial \psi_x}{\partial y}\tau_{xy}\right)\mathrm{d}\Omega - \frac{1}{\rho}\int_\Gamma H\psi_x(\tau_{xx} n_x + \tau_{xy} n_y)\,\mathrm{d}\Gamma = 0, \tag{12}$$

$$W_{q_y} = \int_\Omega \psi_y \left(\frac{\partial (pq_y)}{\partial t} + \frac{\partial}{\partial x}\left(\frac{q_y q_x}{H}\right) + \frac{\partial}{\partial y}\left(\frac{q_y q_y}{H}\right) + c^2 \frac{\partial h}{\partial y} + C_f^b |q| q_y - C_f^s |w| w_y + f_c q_x\right)\mathrm{d}\Omega + \frac{1}{\rho}\int_\Omega H\left(\frac{\partial \psi_y}{\partial x}\tau_{yx} + \frac{\partial \psi_y}{\partial y}\tau_{yy}\right)\mathrm{d}\Omega - \frac{1}{\rho}\int_\Gamma H\psi_y(\tau_{yx} n_x + \tau_{yy} n_y)\,\mathrm{d}\Gamma = 0. \tag{13}$$

The global continuity requirements are for Φ, Ψ, $\boldsymbol{q}$ and h to belong to C^0, the space of functions with continuous values; more precisely, they have to belong to H^1, the space of square integrable functions ; but we have $C^0 \subset H^1$ and C^0 is more manageable.

The boundary integrals arising from the integration by part are called the natural boundary conditions of the system and are obviously influenced by the choice of the formulation. For instance, the boundary term associated to W_h in (11) is ignored on a solid boundary to satisfy the impermeability conditions; it is more comfortable to use this condition than a Dirichlet condition $q_n = 0$ for large simulation involving complex geometry [7]. Also, instead of imposing h that could be in certain cases a constrained condition threatening the convergence of the solution procedure, the known global discharge Q (14)

$$Q = \int_{\Gamma_{in}} q_n \mathrm{d}\Gamma \quad \text{on} \quad \Gamma_{in} \tag{14}$$

can be prescribed as a solicitation in the matrix formulation through $W_h^{\Gamma_{in}}$ on the inflow boundary Γ_{in}. The boundary terms $W_{q_x}^{\Gamma}$ and $W_{q_y}^{\Gamma}$ in (12) and (13) are discretized where the stresses components on Γ are computed with respect to (5).

4. Drying–wetting model

A new Eulerian method is used for the prediction of drying–wetting areas. The choice of the Eulerian approach is motivated by the fact that it is naturally adapted to the physical context. Eq. (1) is used both for the mass conservation and the computation of wet and dry areas through the water level function h. Another approach would be to track the shoreline with a

transport equation [5] resulting in a possibly unstable hyperbolic equation as opposed to the stable parabolic continuity Eq. (1).

In the treatment of the moving boundary, we assume three criteria. First, no condition or limitation is set on the free surface position which can plunge under the bed level and generate positive and negative water depths. Second, the sign convention adopted gives positive depth for wet area and negative depth for dry area. Third, for simplicity, a steady-state flow is assumed in the dry area to control the mass conservation.

Now, we would like to focus on an interesting mathematical property of the variational formulation. In the stationary case, neglecting Coriolis forces and wind stresses, the weak variational forms in (12) and (13) are paired in function of the water depth H

$$W_{q_x}(H) = W_{q_x}(-H) \quad \text{and} \quad W_{q_y}(H) = W_{q_y}(-H). \tag{15}$$

According to Eq. (15), it means that the mathematical model is able to reproduce the same problem with either negative or positive water depths H (Fig. 4). On the other hand, the model cannot distinguish between the wet and the dry area. This also means that theoretically and computationally, water continues to flow in the two types of areas which is in contradiction with the physics.

Starting from this mathematical property, the basic idea is to drive the flow from the dry area ($H < 0$) to the wet one ($H > 0$). Considering the characteristics of flows in rivers, it is well known in hydrodynamics that the major contributions in equations of motion (2) are given by the global equilibrium between the free surface level and the friction terms. In order to respect the principles of mass and momentum conservation in the wet area, we adapt the original mathematical model. The goal is to freeze in the dry area the steady-state flow ($p = 0$) generated by the free surface slope. To achieve this, the action of the *sympathetic* friction operator is increased through a modification of the friction coefficient n based on the depth value H (Fig. 5). In the wet area, the Manning coefficient in (16) and (17) is set in accordance with local flow resistance properties

$$n_{H \geqslant 0} = n. \tag{16}$$

However in the dry area, n varies linearly as a function of H as follows:

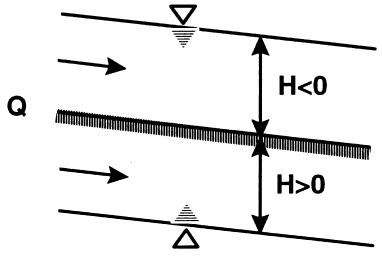

Fig. 4. Flow with positive and negative depth.

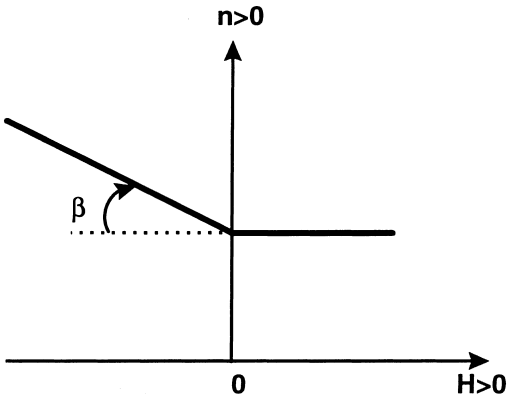

Fig. 5. Variation of Manning coefficient n with the sign of water depth H.

$$n_{H<0} = n(1 + \beta|H|), \tag{17}$$

where n is the classical Manning coefficient related to bed roughness.

Programming this approach in a finite element code is easy and does not require a diagnostic test for numerical efficiency. From the several check tests for stability during the development of the proposed approach, it seems that accuracy is higher at greater β values, but the cost of calculation is much greater. Hence, in practice it is found that the damping coefficient β is in the range $10^2 - 10^4$.

The porosity p of the field is equal to 1 in the wet area and 0, for the steady-state condition, in the quasi-dry area

$$p_{H \geqslant H_{\min}} = 1 \quad \text{and} \quad p_{H<H_{\min}} = 0, \tag{18}$$

where $H_{\min}$ is a positive constant presented later in Section 5.

5. Finite element model

In this section, we present the finite element model for the hydrodynamic simulation of free-surface flows in rivers and estuaries with moving boundaries.

5.1. Stabilization of the weak form

It is well known in the numerical simulation of fluid that the Galerkin finite element method is subject to oscillations in the case of advection-dominated flow. The oscillations can be removed by severe mesh refinement which compromises the appeal of the method, or fortunately by adding a stabilizer smoothing the solution. In this work, the stabilizer is based on a diffusion operator which vanishes with mesh refinement; it is designed to find a solution to a numerical problem without changing broadly the physical phenomenon to modelize.

For instance, the advection operator in (12) and (13) is stabilized on Ω by numerical isotropic viscosity κ^e in (19)

$$\kappa^{\mathrm{e}} = \left|\frac{q}{H}\right|\frac{\Delta^{\mathrm{e}}}{Pe} \quad \text{and} \quad \Delta^{\mathrm{e}} = \sqrt{\int_{\Omega^{\mathrm{e}}} \mathrm{d}\Omega^{\mathrm{e}}} \tag{19}$$

constant per element (C^{-1} approximation) and driven by the Peclet number [11,24]. This numerical viscosity, important but not critical, decreases with the local mesh size Δ^{e} leading to the discretization of the original mathematical model. For the representation of the local mesh size Δ^{e}, we choose the square root of the area of the elementary domain, where the superscript e denotes the element. In practice, the Peclet number is fixed at a value of 0.5.

In addition, to prevent oscillations of the free surface during the solution procedure only, because the shallow water Eqs. (1) and (2) are based on a hydrostatic pressure assumption and are thus limited to flows with small water surface slope, the weak form (11) is stabilized with a second order diffusion operator

$$W_h = W_h + \int_{\Omega} \gamma \left(\frac{\partial \Phi}{\partial x}\frac{\partial h}{\partial x} + \frac{\partial \Phi}{\partial y}\frac{\partial h}{\partial y} \right) \mathrm{d}\Omega. \tag{20}$$

The sensor parameter γ in (20) is in the form of Lapidus [9,14] as follows:

$$\gamma = \gamma_0 (\Delta^{\mathrm{e}})^2 \sqrt{\left(\frac{\partial h}{\partial x}\right)^2 + \left(\frac{\partial h}{\partial y}\right)^2}, \tag{21}$$

where γ_0 is a constant value in the range of 10^{-5} and Δ^{e} is the local mesh size. γ is constant per element and acts only in the region of high gradient of the free surface. Neglecting the boundary term naturally associated with the diffusion operator in (20) implies the following boundary condition on the water level

$$\frac{\partial h}{\partial x} n_x + \frac{\partial h}{\partial y} n_y = 0 \text{ on } \Gamma. \tag{22}$$

Another point related to the stability of the model is the singularity that occurs along the shoreline where $H = 0$. To avoid locking up the computational procedure, the water depth is corrected as follows:

$$\tilde{H} = \max(H_{\min}|H|). \tag{23}$$

In addition, the weak variational forms (12) and (13) are stabilized by the use of the absolute value of water depth H

$$W_{q_x} = W_{q_x}(\tilde{H}) \text{ and } W_{q_y} = W_{q_y}(\tilde{H}), \tag{24}$$

where the value of $H_{\min}$ in (23) is generally fixed at 10^{-3} m. In fact, using $\tilde{H}$ reduces the variation of the velocity along the normal direction to the shoreline, minimizing at the same time the advection phenomenon which helps the convergence procedure.

5.2. Finite element approximation

In the development of stable finite elements for shallow water models, it is conventional to choose a richer approximation for $\boldsymbol{q}$ or $\boldsymbol{u}$ than for h [2,6,23]. The work of Babuska [1] and Brezzi [3] for mixed finite element models has led to the definition of consistency conditions for Stokes flows. Not respecting the Brezzi–Babuska condition (called BB or inf–sup condition) leads to spurious oscillations of water level values which then pollute the field of $\boldsymbol{q}$ or $\boldsymbol{u}$ [4].

We use the linear 6-node triangular element called *T6L* [25], which is a combination of 4 identical 3-node linear triangular elements *T3* in order to respect the BB condition, to represent the flow variables and the computational domain Ω. We use the approximation known as 'P_1, P_1 *iso* P_2' where the specific discharge has the same number of degrees of freedom as with a P_2 approximation (with P_k the space of polynomials of degree k).

Spatial approximations for water level h and specific discharge $\boldsymbol{q}$ have a C^0 continuity and are represented on a reference element (Fig. 6). We use a linear approximation for h and Φ on the main triangle. We encounter the natural relationship $h_i = 1/2(h_{i+1} + h_{i-1})$ on the water level between the middle nodes (i) and the vertex nodes ($i+1$ and $i-1$). We have the same approximation as h for the water depth $\tilde{H}$ and the bed topography z_{f}. For $\boldsymbol{q}$ and Ψ, the approximation is linear on each *T3* sub-triangle, and we have a piecewise linear approximation on the main triangle *T6L*.

The expressions of the linear shape function N and its derivatives on a reference element *T3* are as follows:

$$\langle N \rangle = \langle 1-\xi-\eta\,;\,\xi\,;\,\eta \rangle \mapsto 0 \leqslant \xi \leqslant 1\,;\, 0 \leqslant \eta \leqslant 1,$$
$$\begin{bmatrix} \langle N_{,x} \rangle \\ \langle N_{,y} \rangle \end{bmatrix} = \frac{1}{\det j} \begin{bmatrix} (y_2-y_3) & (y_3-y_1) & (y_1-y_2) \\ (x_3-x_2) & (x_1-x_3) & (x_2-x_1) \end{bmatrix}, \tag{25}$$

where the $\boldsymbol{x}_i(x_i,y_i)$ are the coordinates of the nodes and det j is the determinant of the Jacobian of the geometrical transformation from real to reference element:

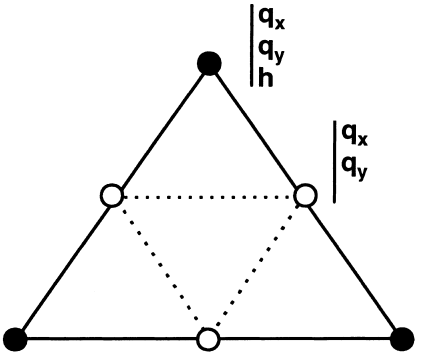

Fig. 6. Finite element *T6L*.

$$\det j = (x_2 - x_1)(y_3 - y_1) - (x_3 - x_1)(y_2 - y_1) > 0. \quad (26)$$

The variables $\boldsymbol{q}$ and h and the respective test functions are approximated on a reference element $T3$ as follows:

$$\begin{aligned} &q_x = \langle N\rangle\{q_{x_n}\}; q_y = \langle N\rangle\{q_{y_n}\}; \;\; h = \langle N\rangle\{h_n\}, \\ &\psi_{q_x} = \langle N\rangle^{\mathrm{T}}; \psi_{q_y} = \langle N\rangle^{\mathrm{T}}; \;\; \Phi = \langle N\rangle^{\mathrm{T}}, \end{aligned} \quad (27)$$

where the subscript n denotes the nodal value.

To discretize the advection, diffusion and friction operators in (12) and (13) we employ the factored product commonly used in finite difference or finite volume [21]. Fixing the ideas, for example the discretized form of the advection operator, using Einstein's notation, leads to the following expression:

$$\int_{\Omega^e} \psi_{q_{x_i}} \frac{\partial}{\partial x_j}\left(\frac{q_{x_i} q_{x_j}}{H}\right) \mathrm{d}\Omega^e \to \int_{\Omega^{\mathrm{ref}}} \langle N\rangle^{\mathrm{T}} \langle N_{,x_j}\rangle \times \left\{\frac{q_{x_{in}} q_{x_{jn}}}{H_n}\right\} \det j \, \mathrm{d}\Omega^{\mathrm{ref}} \quad i = 1,2; \;\; j = 1,2. \quad (28)$$

As long as $\boldsymbol{q}$ and h vary linearly, in accordance to the choice of approximation (25)–(27), the numerical model reproduces an exact linear solution under the condition where the water depth remains constant because it appears in $1/H$ in advection and diffusion operators in (12) and (13).

5.3. Matrix formulation

The spatial discretization of the stabilized weak variational forms (20) and (24), by the finite element approximation (25)–(27), combined with an implicit Euler scheme to approximate time derivatives, led to an algebraic nonlinear set of equations written as follows:

$$\{\boldsymbol{R}\} = [\boldsymbol{M}](\{p\boldsymbol{U}\}_{t+\Delta t} - \{p\boldsymbol{U}\}_t) + \Delta t([\boldsymbol{K}(\boldsymbol{U})]\{\boldsymbol{U}\} - \{\boldsymbol{F}\})_{t+\Delta t}, \quad (29)$$

where $[\boldsymbol{M}]$ is the symmetric mass matrix, $[\boldsymbol{K}]$ the rigid nonsymmetric and nonlinear matrix and $\{\boldsymbol{F}\}$ and $\{\boldsymbol{R}\}$ are the solicitations and the residual vectors, respectively. In (29), Δt denotes the time step and the nodal porosity parameter p is computed according to (18) at time $t + \Delta t$. The subscripts t and $t + \Delta t$ indicate the referenced times.

The role of the resolution procedure is to find $\{\boldsymbol{U}\}$, the vector of all degrees of freedom, at $t + \Delta t$, assuming that it is known at t. It must satisfy the condition $\{\boldsymbol{R}(\boldsymbol{U})\} = \{\boldsymbol{0}\}$, but in practice the convergence is achieved until the norm of the residual is small enough. The resolution procedure is worked out with a nonlinear version of GMRES [20,21] using Incomplete Lower-Upper (ILU) factorization as preconditioning [15]. This solver does not require the storage of a large matrix; which is interesting when it deals with many degrees of freedom.

6. Numerical results

In this section, we present the results obtained with this approach in modeling moving boundaries. In the first example, a steady-state flow with an analytical solution is proposed. In the second case, we reproduce a time-dependent solution. In the last example, we apply our model to an experimental case. In these examples, the Coriolis and wind forces are ignored. All the calculations were performed with a FORTRAN 77 code in double precision.

6.1. Flow in channel with triangular cross section

To assess the quality of the new method in modeling moving boundaries in a two-dimensional free surface flow, we established a benchmark example. We considered a channel with a triangular cross section where the wet area is defined by the surface ($ABCD$) and the dry area by the surface ($ABC'D'$). The boundary separating the two areas is defined by x axis for $y = 0$ (Fig. 7).

Assuming no flow in the transverse direction y, free surface slope equal to i_b and neglecting the advection terms, the wind and the Coriolis forces in (2), we arrive at the following reduced form for conservation of momentum

$$gH\frac{\partial h}{\partial x} - \frac{1}{\rho}\frac{\partial}{\partial y}(H\tau_{xy}) + \frac{n^2 g|q|q_x}{H^{7/3}} = 0. \quad (30)$$

The law of the depth variation is as follows:

$$H(y) = my \quad (31)$$

and the linear solution of the water level h is as follows:

$$h(x) = i_b x. \quad (32)$$

Integrating the equation of momentum (30) along the y axis from $y = 0$ to $y = l$ and considering the boundary conditions

$$H(y=0) = 0 \quad \text{and} \quad \frac{\partial}{\partial y}\left(\frac{q_x}{H}\right)\Big|_{y=l} = 0,$$

we obtain

$$v_t H \frac{\partial}{\partial y}\left(\frac{q_x}{H}\right)\Big|_0^l = \int_0^l \left(gH\frac{\partial h}{\partial x} + \frac{n^2 g|q|q_x}{H^{7/3}}\right)\mathrm{d}y = 0. \quad (33)$$

Replacing in (33) the water depth H by (31) and $\partial h/\partial x$ by the derivation of (32), we obtain the following expressions for the specific discharge q_x

$$q_x(y) = \frac{1}{n}\sqrt{|i_b|}(my)^{5/3} \quad (34)$$

the velocity u

$$u(y) = \frac{q_x}{H} = \frac{1}{n}\sqrt{|i_b|}(my)^{2/3}. \quad (35)$$

The simulation procedure was conducted with regular triangular elements (Fig. 8) and various mesh sizes

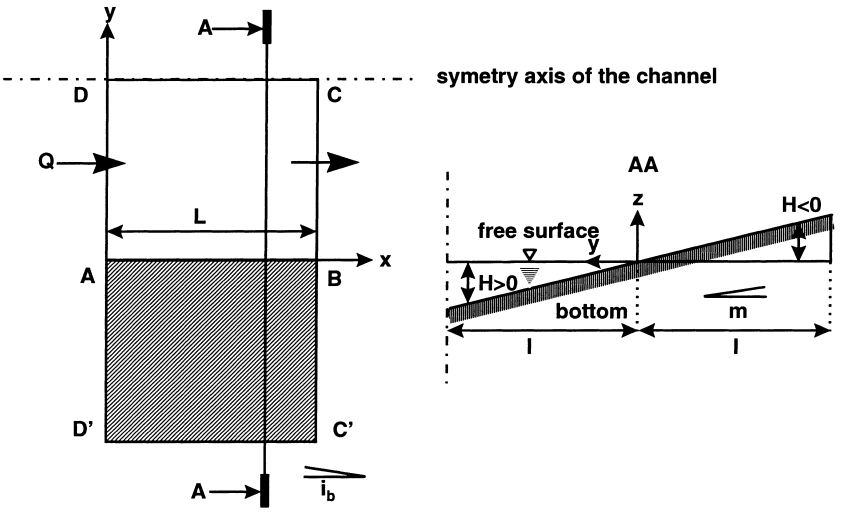

Fig. 7. Channel with triangular cross section: geometry.

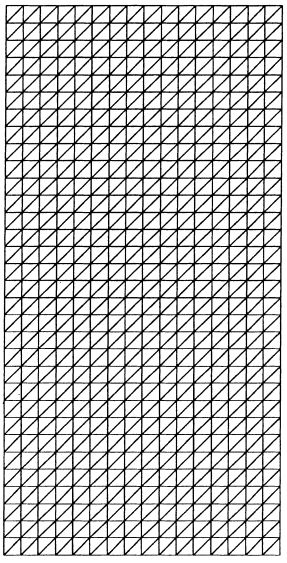

Fig. 8. Channel with triangular cross section: 16×32 *T6L* elements.

(1×2, 2×4, 4×8, 8×16 and 16×32 elements) in order to study the rate of convergence. Although the configuration of these several meshes assumes that the position of the shoreline ($H = 0$) is located along the boundary of interested elements, numerical tests with meshes having an impair number of elements along the y-axis direction prove that we obtain the same results when the shoreline crosses the elements.

The channel is $L = 12.0$ m long, $l = 12.0$ m wide and has a 1.5 m mean depth. The longitudinal bed slope $i_b = -3.19554 \times 10^{-3}$ m/m in the x-axis direction and the transversal slope $m = 0.125$ m/m in the y-axis direction (Fig. 7). The kinematic viscosity, the Manning n of the bed and the gravitational acceleration are given the following respective values: 10^{-6} m^2/s, 0.02 and 9.806 m/s^2. Thus, the value of the global discharge Q_0 is:

$$Q_0 = \int_0^l q_x(y)\,\mathrm{d}y = \frac{3}{8n}\sqrt{|i_b|}(m^5 l^8)^{1/3} = 25.00\ \mathrm{m}^3/\mathrm{s}. \tag{36}$$

The numerical parameters γ_0 and κ^e were turned off and $H_{\min}$ was fixed at 1.0×10^{-3} m. Water level values were specified on the face (DD') ($h = 0$) and on the face (CC') ($h = -0.03835$ m). On this latter face, $q_t = 0$ was also prescribed. On ($C'D'$) and (CD), impermeability in weak form ($W_h^{(C'D')} = W_h^{(CD)} = 0$ and q_n free) has been used. For the initial condition, we use the static solution ($q_x = q_y = h = 0$). The discrete L_2 norm of convergence of the iterative process has been limited to

$$\|\{\boldsymbol{R}(\boldsymbol{U})\}\|_0 = 10^{-6},$$

where the discrete L_2 norm of a given vector $\boldsymbol{F}$ is defined as follows:

$$\|\boldsymbol{F}\|_0 = \frac{1}{k}\sqrt{\langle \boldsymbol{F}\rangle\{\boldsymbol{F}\}} \quad k = \dim(\{\boldsymbol{F}\}). \tag{37}$$

Fig. 9a shows the regularity of the isobars and the boundary separation ($H = 0$) between the dry and wet areas. The water level coincides practically with the exact solution given by (32). Fig. 9b shows clearly that velocity vectors vanish for the dry area ($H < 0$) and mass conservation is better for greater β values (Figs. 10 and 11), in accordance with the equilibrium of hydrostatic and friction forces in (30). The discharge Q_d in the dry area decreases rapidly with an increase of the parameter β. However the maximum value of Q_d does not exceed 0.6% of Q_0 (Fig. 11).

In Fig. 12, we have the same curve of the discrete L_2 norm (Eq. (37)) error in the wet area between the finite element solution q_x and the exact solution q_{ex} (Eq. (34)). versus mesh size h. Moreover, the slope of the curve indicates a quadratic convergence of the variable q_x which is in accordance with the theory. It was obtained

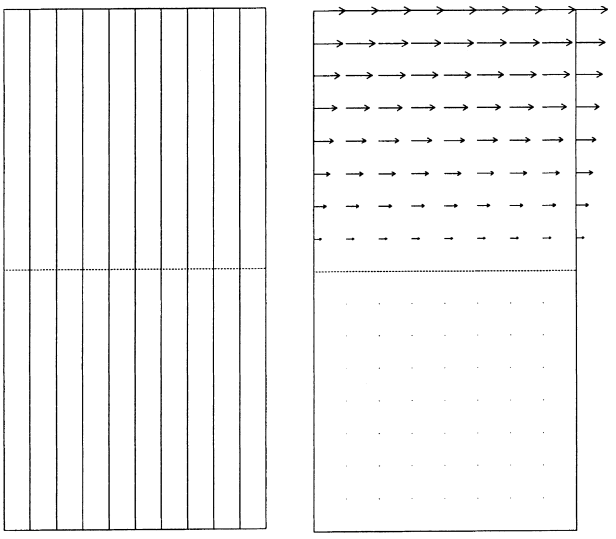

Fig. 9. Channel with triangular cross section: (a) water levels; (b) velocity field.

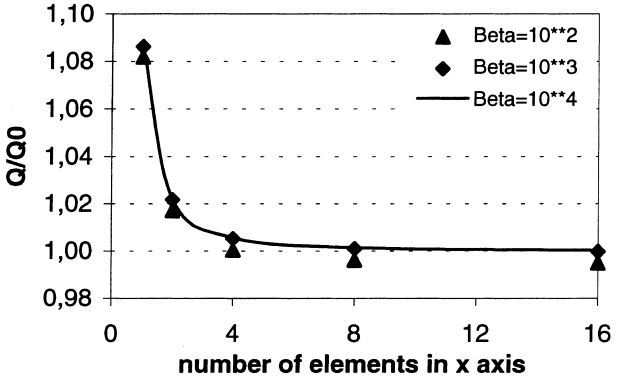

Fig. 10. Channel with triangular cross section: variation of Q with mesh size for various values of β.

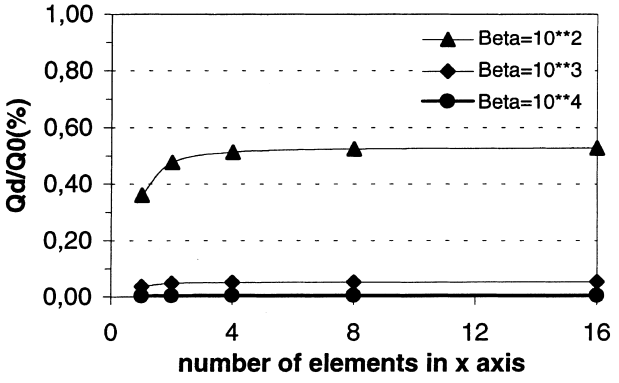

Fig. 11. Channel with triangular cross section: variation of Q_d in the dry area for various values of β.

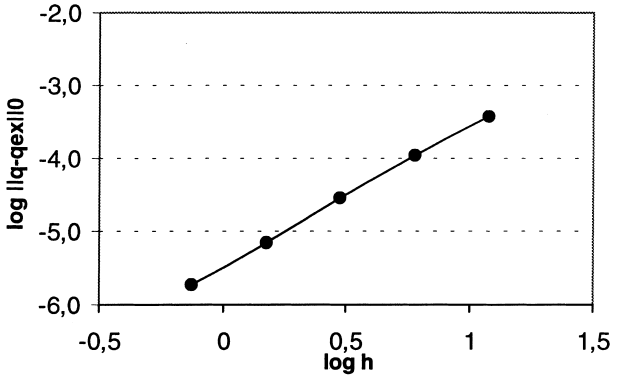

Fig. 12. Channel with triangular cross section : variation of q_x L_2 norm error with mesh size h.

with several values of β (10^2, 10^3, 10^4). From this result, we inferred that the dry area does not influence the flow in the wet area for large β values, and the principles of conservation of mass and momentum are satisfied.

6.2. Basin with a variable slope under a tidal cycle

For the time-dependent solution, we encounter an interesting situation where we have two kinds of equations of conservation : time dependent in the wet area and steady state in the dry area. This example was proposed initially by Leclerc et al. [17] in order to reproduce the shoreline movement under a tidal cycle in a rectangular channel with a variable slope (Fig. 13a). The channel is 500 m long and 25 m wide. The slope i_b in the longitudinal direction and the bed topography are defined in Table 2.

The domain is discretized with 35 elements, of variable sizes, in the x direction and five elements in the y direction (Fig. 13b) Impermeability conditions are specified on solid boundaries (AB), (CD) and (DA). On the open boundary (BC), $q_t = 0$ and the water level h varies with the tide cycle

$$h = h_0 + \eta \cos\left(2\pi \frac{t}{T}\right), \tag{38}$$

where h_0 is the reference water level, η the amplitude and T the period of the tidal cycle, being 1.00 m, 0.75 m and 60 min, respectively. As initial conditions, static solutions $q_x = q_y = 0$ and $h = 1.75$ m were imposed at time $t = 0$. We used a fully implicit Euler scheme with a time increment Δt of 3 min. The wind and the Coriolis forces are neglected in Eq. (2). The friction coefficient n, the constant kinematic viscosity v_t and the porosity p are given the following respective values: 0.03, 5.0 m^2/s and 0.0.

The results are shown in Fig. 14 for several time steps during one drying–wetting cycle. One can observe that the model is able to reproduce the movement of the shoreline. In the dry area, the velocity vanishes and the

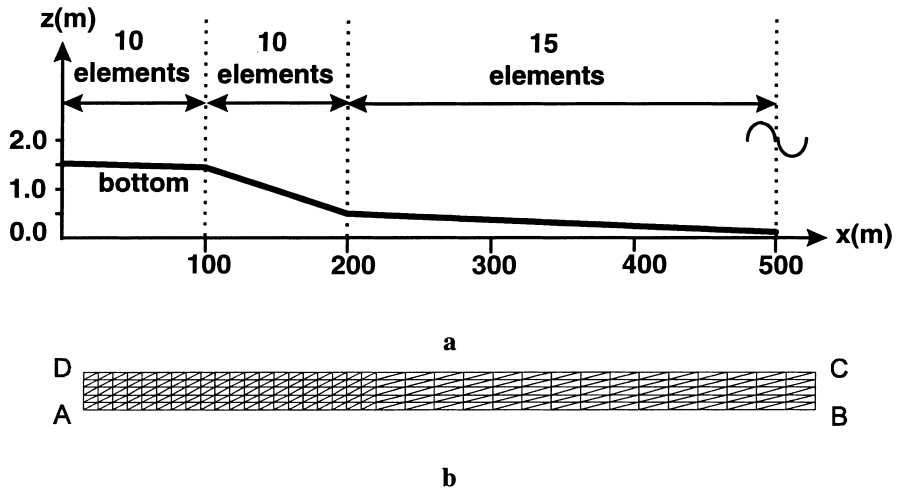

Fig. 13. Basin with a variable slope: (a) geometry; (b) mesh.

Table 2
Basin with variable slope: bed topography data

x (m)	0–100	100–200	200–500
i_b (m/m)	-10^{-3}	-10^{-2}	-10^{-3}
z_f (m)	1.4–1.3	1.3–0.3	0.3–0.0

water surface level is constant (equations of motion (2) reduced to $\partial h/\partial x \approx 0$) and takes the value of the intersection point with the bottom ($H = 0$).

In the dry area, the results were influenced by the $H_{\min}$. The portion of the channel where $x < 200$ m is never empty for small $H_{\min}$ values. As a consequence, beginning at $t = 12$ min we encounter a very shallow depth that occurs at hard numerical hydraulic conditions because of the spurious oscillations of the water surface level of the same order of magnitude as the depth values, and also of a significant acceleration of the velocities which dominates the flow for 100 m $< x <$ 220 m. To stabilize the solution procedure and to avoid the oscillations generated by the material non linearity, especially in the region where $i_b = -10^{-2}$ m/m, we used values of $\gamma_0 = 10^{-5}$ and $Pe = 0.5$. To obtain a similar solution to Leclerc et al. [17], $H_{\min}$ and β were fixed at 5.0×10^{-2} m and 10^2, respectively.

6.3. Ashuapmushuan river (Québec, Canada)

The present model was applied to study the steady-state current in the Ashuapmushuan River (km 70). This study is part of a research project on fish habitats [16]. This natural field is characterized by a curved geometry, a complex bed topography and a variable friction coefficient. The wind and the Coriolis forces are neglected because they are not of importance. The objective is to qualitatively compare the relevance of our new approach with the classical one in modeling moving boundaries under actual field conditions.

The mesh used is presented in Fig. 15 and has 1659 elements *T6L* and 3444 nodes corresponding to 10 332 degrees of freedom. The physical parameters λ in (6) for variable turbulent kinematic viscosity v_t and Manning coefficient are given the following values: 1.0, 0.023–0.038. The numerical parameters Pe, $H_{\min}$, β and γ_0 were fixed at 0.5, 1 mm, 10^2 and 0, respectively. We specify the water level on the outflow boundary (*BC*) and impermeability conditions on solid boundaries (*AB*) and (*CD*). On the inflow boundary (*AD*), we also specify the water level and the direction of the flow ($q_t = 0$). The boundary conditions prescribed correspond to a dry-weather flow event ($Q = 73$ m^3/s). For the initial conditions, we specify hydrostatic conditions ($q_x = q_y = 0, h =$ constant). The problem was solved on a P.C. pentium 133 MHz and requires 7 Mb of space on memory. The strategy of resolution employed was based on a gradual fall of the water level at inflow boundary with an increment of 30 cm; thus nine steps were required to achieve the total unevenness of 2.38 m between the inflow and outflow boundaries. Finally, the problem was converged in 180 min with a tolerance of 10^{-7}.

The results obtained are qualitatively compared with those of the classical approach computed earlier as a reference solution, on a MICROVAX 3+ computer, with a direct method and the same strategy as presented above; however the increment was of only 3 cm, ten times smaller. The comparison of the results aims at checking the position of the natural boundaries of the flow, and also if the velocity vectors vanish in the dry area. On a graphic interface, the shorelines are obtained by displaying the contour lines $H = 0$. Fig. 16a and b illustrate the boundary of the mesh, contour lines for $H = 0$ and velocity vectors that vanish in the dry area, obtained with the classical approach (a) and the new approach (b). One can observe that the results of the new approach are in very

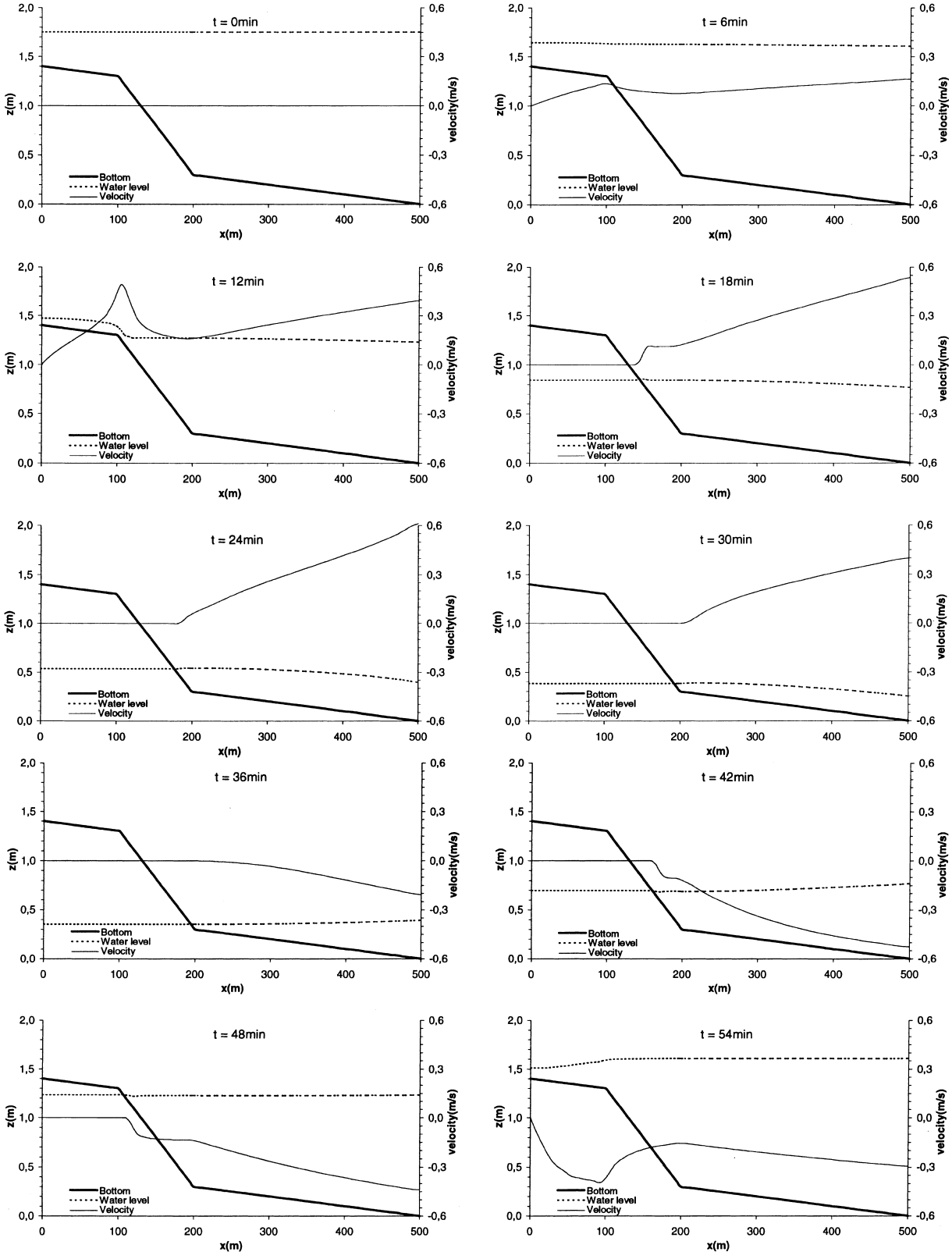

Fig. 14. Basin with a variable slope: variation in time of velocity and water level.

good agreement with the classical one. The maximum differences are located in the shallow water area combined with a high bed slope. Thus, a small difference on water level between the two approaches produces locally slight differences in the position of the shoreline.

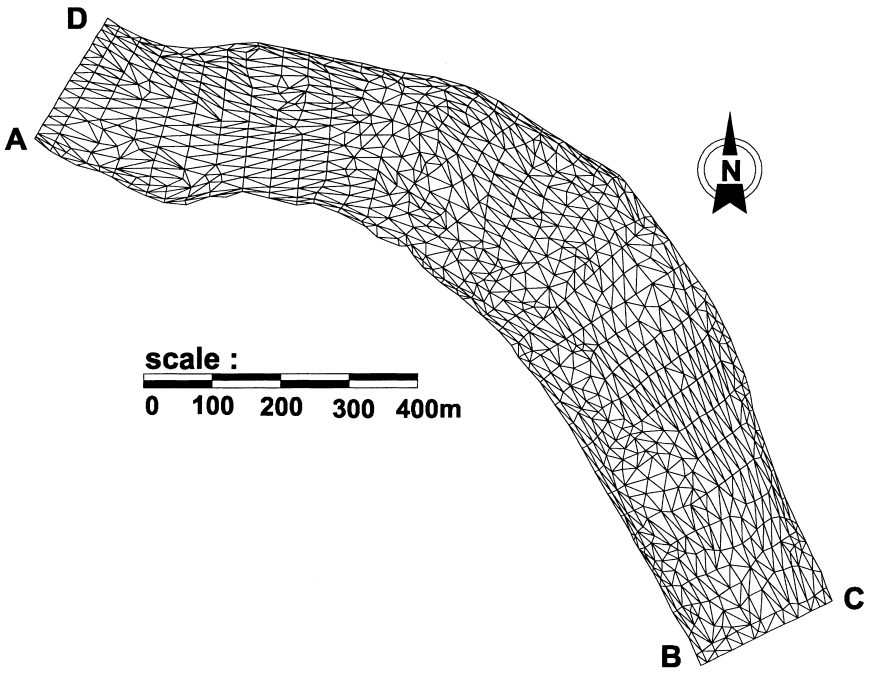

Fig. 15. Ashuapmushuan River: mesh (1659 elements, 3444 nodes).

7. Conclusion

A new approach in hydrodynamics for the simulation by the finite element method of the moving boundaries of flows on a horizontal plane has been presented. No assumption is made on the water level position which is free to plunge under the immobile bottom. Thus it is possible to encounter positive and negative water depth values (Fig. 1) where the convention sign indicates a dry or a wet area, when the depth value is negative or positive respectively. This method is general enough to reproduce complex profile of the shoreline either in stationary or transient flow modeling. The continuity and the momentum in discrete form are fully conserved on the entire domain of simulation and allow for the realistic calculation of the velocity profiles in wet areas; and the flow is frozen with a relatively high friction coefficient in the dry areas. Applied on several real cases, with large zones undergoing drying and wetting, the method proved its accuracy and robustness. But more work must be done to evaluate the method in the case of rapid boundary movement produced by either a dam break or by a short frontal tidal wave; in these situations [17], the classical approach does not perform.

Three positive points are retained which demonstrate the advantage of the present approach over the classical approach: the principles of conservation are fully satisfied on wet elements, there is no fictitious free surface slope on transition elements, which is undesirable for applications based on hydrodynamic data, and especially the ease of programming. Indeed, the most important feature of the proposed method is its simplicity, in comparison with the classical approach, which is a significant asset for future development within the framework of a policy software. The question of the speed of run is most related to the solver to be used. The choice of a GMRES type solver, despite the fact that it requires a certain experience of use, is justified not only for its well-known speed, but also for its robustness to absorb the strong variation of the friction between dry and wet areas; it is also more flexible to use for large problems and less expensive in memory requirements than the direct method.

In practice, the application of the proposed approach in complex open channel flow computations is dedicated, among other things, to the analysis of extreme flood and tidal wave propagation, the delimitation of flood plain in function with the frequency of the discharge, and the influence of the hydraulic management on the flow. The hydrodynamic results can be used a posteriori in the estimation of flood damages under the submersion depth, in the study of fish habitats, in the monitoring of the development of aquatic vegetation, and the transport of pollutants, sediment and ice.

Acknowledgements

The authors would like to acknowledge the financial support of Ministère de l'Environnement et de la Faune (Québec) for this work. Finally, the authors gratefully thank Mr. Ronald Greendale for his review of the present paper.

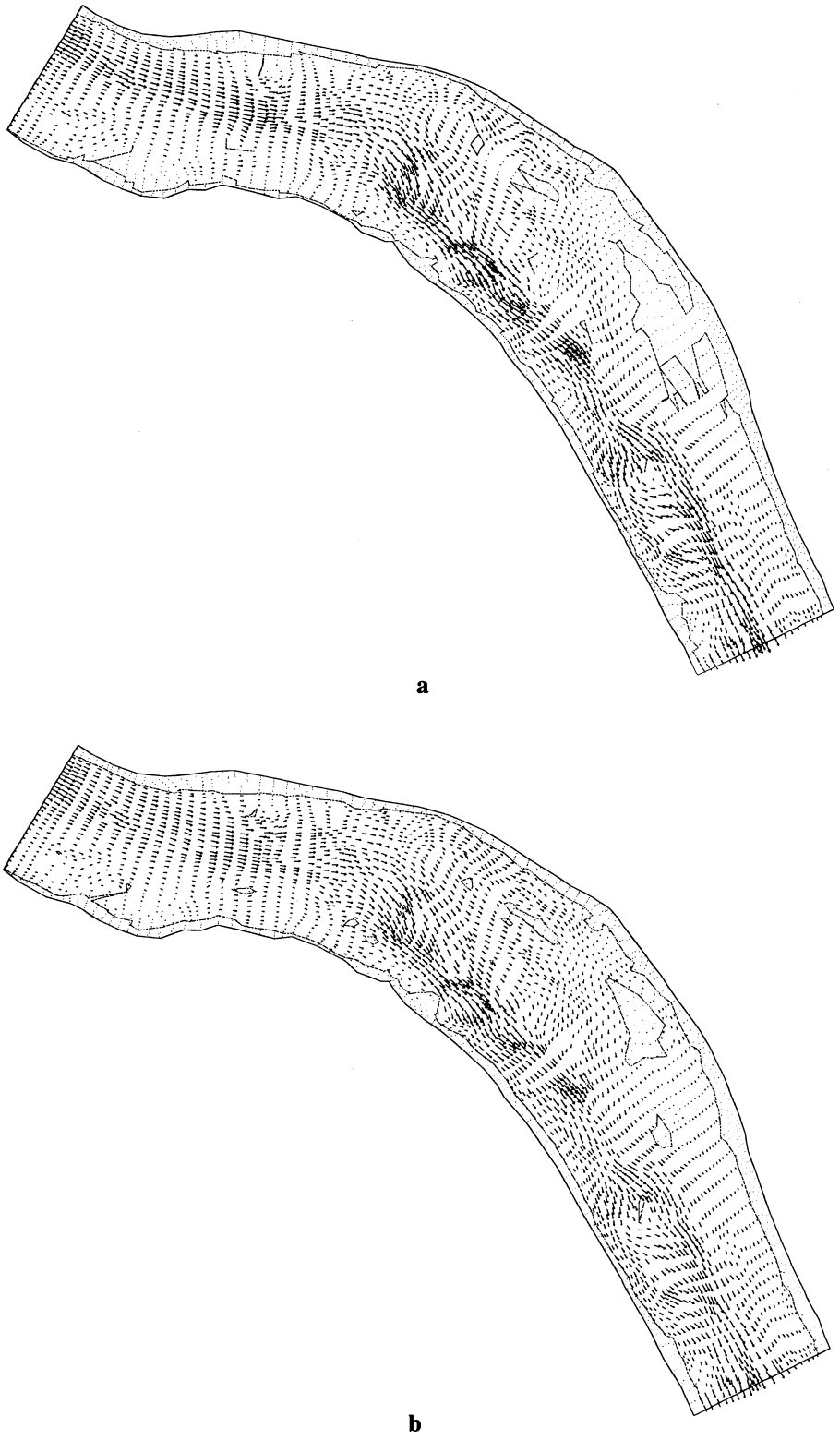

Fig. 16. Ashuapmushuan River: velocity and bed configuration. (a) classical approach; (b) new approach.

References

[1] Babuska I. Error bounds for finite element method. Num Math 1971;16.

[2] Bercovier M, Pironneau O. Error estimates for finite element method solution of the Stokes problems in the primitive variables. Num Math 1979;33.

[3] Brezzi F. On the existence, uniqueness and approximation of saddle point problems arising from Lagrange multipliers. RAIRO, Série Rouge 1974;R2:129–51.

[4] Connor JJ, Wang JD. Finite element modelling of hydrodynamic circulation. In: Brebbia CA, Connor JJ, editors. Num Meth in Fluid Dynamics. Plymouth: Pentech Press, 1974.

[5] Dhatt G, Gao DM, Bencheick M. A finite simulation of metal flow in moulds. IJNME 1990;30:821–31.

[6] Dhatt G, Soulaimani A, Ouellet Y, Fortin M. Development of new triangular elements for free surface flows. IJNMF 1986;6:895–911.

[7] Galland JC, Goutal N, Hervouet J-M. TELEMAC: a new numerical model for solving shallow water equations. Advances in Water Resources 1991;14:138–48.

[8] Ghanem AHM. Two-dimensional finite element modeling of flow in aquatics habitats. Ph.D. Thesis, The University of Edmonton, Alberta (Canada), 1995.

[9] Heniche M. Modélisation tridimensionnelle par éléments finis d'écoulements à surface libre. Ph.D. Thesis, Université de Technologie de Compiègne, France, 1995.

[10] Holz K-P, Nitsche G. Tidal wave analysis for estuaries with intertidal flats. Advances in Water Resources 1982;5:142–8.

[11] Hughes TJR, Brooks A. A multi-dimensionnal upwind scheme with no crosswind diffusion. In: Hughes TJR, editor. Finite Element Methods for Convection Dominated Flows, ASME, New York, 1979.

[12] Jansen Ph, Van Bendegom L, Van den Berg J, de Vries M, Zanen A. Principles of rivers engineering. The non tidal alluvial river. London: Pitman, 1979.

[13] Kawahara M, Umetsu T. Finite element method for moving boundary problems in river flow. IJNMF 1986;6:365–86.

[14] Lapidus A. A detached shock calculation by second order finite difference. J Comput Phys 1967;2:154–77.

[15] Leclerc M, Secretan Y, Heniche M, Roy Y. Projet MÉTRIQUE: Bilan scientifique. Rapport d'étape #3 au Fonds de recherche et de développement technologique en environnement (MEF). Report INRS-Eau R482, 1996.

[16] Leclerc M, Boudreau P, Bechara J, Corfa G. Modélisation de la dynamique de l'habitat des ouananiches (Salmo salar) juvéniles de la rivière Ashuapmushuan (Québec Canada). Report INRS-Eau R482, 1994.

[17] Leclerc M, Bellemare J-F, Dumas G, Dhatt G. A finite element model of estuarian and river flows. Advances in Water Resources 1990;4:158–68.

[18] Lynch DR, Gray WG. Finite element simulation of shallow water problems moving boundaries. Finite Elements in Water Resources. In: Proceedings of the Second International Conference on F.E. in Water Resources. London: Pentech Press, July 1978.

[19] Rodi W. Turbulence models and their application in hydraulics. State-of-the-art paper, IAHR-AIRH, 1984.

[20] Saad Y, Schultz MH. GMRES: a generalized minimal residual algorithm for solving non symmetric linear systems. SIAM J. Sci. Stat. Comp. 1986;7(3):856–69.

[21] Secretan Y. Un schéma élément fini simple et adaptatif pour les écoulements de Navier-Stokes compressibles. A simple and adaptative finite element scheme for the compressible Navier–Stokes flows. Revue Européenne des Éléments Finis 1992;1(1):31–50.

[22] Shanahan P, Harleman DRF. Linked hydrodynamic and biochemical models of water quality in shallow lakes. Report 268, Ralph Parson Lab. Cambridge, MA: MIT Press, 1982.

[23] Taylor C, Hood P. Numerical solution of the Navier–Stokes equations using the finite element technique. Comp and Fluids 1973;1:1–28.

[24] Zienkiewicz OC, Taylor RL. The finite element method, vol. 2, 4th ed. New York: Mc Graw Hill, 1992.

[25] Zhang BN, Bouttes F, Dhatt G. A shallow water finite element model for moving fronts. VIII International Conference on Computational Method in Water Resources, Venice, Italy, 1990.